CHEMISTRY
A EUROPEAN JOURNAL

DOI: 10.1002/chem.200700310

Vibrational Study on the Local Structure of Post-Synthesis and Hybrid Mesoporous Materials: Are There Fundamental Distinctions?

Pedro D. Vaz,*[a] Carla D. Nunes,[a] Maria Vasconcellos-Dias,[a] Mariela M. Nolasco,[b] Paulo J. A. Ribeiro-Claro,[b] and Maria José Calhorda*[a]

Abstract: Organic–inorganic mesoporous materials of the MCM-41 type are important materials that can be prepared by either post-synthesis or one-pot synthesis procedures. A complete control of the characteristics at a local level is of the utmost importance in view of the applications of such materials. However, there are not many studies relating such features with synthetic approaches. In this work, we prepared samples by post-synthesis derivatization of materials from Si-based MCM-41, with bidentate nitrogen ligands bearing one or two silylated arms, and by one-pot synthesis of organic–inorganic hybrid materials. The bulk properties of the two kinds of materials were comparable. Diffuse reflectance infrared Fourier transform (DRIFT) spectroscopy and Raman spectroscopy were used to investigate the local environment, namely, the number of OH groups and distribution of SiO_4 units (large and small ring units). Hydrophilicity correlates with both the type of organic moiety used (mono- or disilylated), as well as with the synthetic procedure. The same vibrational studies showed how the structure in the channels changes as a function of pressure, reflecting the low mechanical stability of the mesoporous materials.

Keywords: IR spectroscopy · mesoporous materials · organic-inorganic hybrid composites · Raman spectroscopy · sol–gel process

Introduction

Inorganic materials based on silica matrices have been used in many fields for miscellaneous applications for some time, though lack of technological and architectural features has restricted their variety. In 1992 a major leap forward occurred with the discovery of the M41s mesoporous material family.[1,2] Since then, numerous papers have contributed decisively to the development of this field, opening new routes for functionalization.[3,4] The main approach for derivatizing such materials was by post-synthesis grafting or tethering procedures of the silica walls. Whereas the former is based on the direct reaction of a suitable silicon derivative with the OH groups on the walls of the material, in the latter, the chosen molecule is introduced with the reagents when synthesizing the material. The tethering approach has enabled the introduction of organic moieties into the inorganic frameworks by the one-pot preparation of hybrid organic–inorganic materials,[5–13] which also offers the advantage of a better distribution of the organic moieties in the walls than achieved with the grafting approach.

Despite these available approaches to engineer new materials and all the improvements introduced, some problems still remain. A relevant question is related to the structural similarities or differences that arise when different synthetic procedures are used, namely whether organic moieties lie at the outer or inner side of the walls. For instance, the grafting process only allows the introduction of the organic moieties at the surface, but the same cannot be said of the tethering process.

It is well documented that in silica gel, the SiO_4 tetrahedral units are arranged not only in the thermodynamically favored siloxane 4-rings, but also in the form of kinetically favored and less strained 6-rings.[14] Recently, state-of-the-art studies addressing the local structure of silica gels showed that the infrared-active Si-O-Si asymmetric stretch appears as a broad band and its frequency is a function of the Si-O-

[a] Dr. P. D. Vaz, Dr. C. D. Nunes, M. Vasconcellos-Dias, Prof. M. J. Calhorda
Department of Chemistry and Biochemistry
CQB, Faculty of Science, University of Lisbon
C8 Campo Grande, 1749–016 Lisboa (Portugal)
Fax: (+351) 217-500-088
E-mail: pmvaz@fc.ul.pt

[b] M. M. Nolasco, Dr. P. J. A. Ribeiro-Claro
Department of Chemistry, CICECO
University of Aveiro
Campus de Santiago, 3810–193 Aveiro (Portugal)

Supporting information for this article is available on the WWW under http://www.chemeurj.org/ or from the author.

Si angle.[14] For this type of material this band comprises both longitudinal-optic (LO) and transversal-optic (TO) modes, more or less separated depending on the degree of long-range interactions.

These LO and TO modes may be interpreted by considering a lattice with two atoms, Si and O, in the unit cell. As their atomic masses are different, both atoms will experience displacements with different amplitudes, due to the different masses. If the displacement is out-of-phase, the modes are called optical modes. In the case of the longitudinal mode (LO), the displacement of atoms away from their equilibrium position is in the same direction as the propagation direction of the wave, whereas for the transverse mode (TO), the atoms move in a direction perpendicular to the direction of the propagation of the wave.

Specific frequencies are expected to arise for each population of ring dimensions, because they correspond to different average Si-O-Si angles, but to the best of our knowledge there are only a few reports on the local structure of silica matrix materials.[14–16] Although several reports have discussed the study of hydroxy groups,[17–21] none of them considered the problem of mesoporous hybrid organic–inorganic materials. Only recently was the study of periodic mesoporous organosilicas (PMOs) by vibrational spectroscopy addressed by Hoffmann and co-workers,[22] who compared experimental data with results of DFT calculations to probe the νSiC modes of several organic building blocks.

Herein a combined vibrational study based on FTIR and FT Raman measurements is performed to address the influence of the synthetic procedure (grafting versus tethering) on the local properties of materials, by using the surface OH groups as a probe. Both the hydrophilicity of a material and its mechanical stability can be rationalized from this study. To carry out the study, two widely used nitrogen bidentate ligands were selected and prepared for the post-synthesis grafting and for the hybrid-material one-pot syntheses. The structures of the ligands are shown in Scheme 1; the main difference is the presence of one silylated side chain in **1** and two in **2**.

Results and Discussion

Chemical studies and characterization: Ligands **1** and **2** bearing the $Si(OEt)_3$ groups were synthesized as described in the Experimental Section.[23] The synthesis of ligand **1** was confirmed by spectroscopic data and elemental analyses.

Two routes were followed to prepare the materials as depicted in Scheme 2. The first route starts with the synthesis of the pure siliceous MCM-41 by a template approach as described previously.[23] Two aliquots of this material were derivatized afterwards by grafting both ligands onto the silica-matrix mesoporous host material, in toluene, overnight. After filtration, the solids were washed thoroughly with dichloromethane, and dried in vacuum at 373 K for several hours.[23] The two materials obtained were denoted PMS_1 and PMS_2, depending on the ligand grafted (**1** or **2**, respectively). This procedure afforded conventional post-synthesis organically modified periodic mesoporous silica.

The same type of material was prepared by the second route, but the organic ligands **1** and **2** were co-condensed with the silica source (TEOS) resulting in a one-pot synthesis procedure. The hybrid materials prepared from ligands **1** and **2** by this method were denoted PMO_1 and PMO_2, respectively. This synthetic route followed the method described by Jia and co-workers,[24] but NaOH was replaced by the weaker base $EtNH_2$, to avoid contamination with Na^+ ions in the final mesoporous material. In the course of the synthesis, methanol was used as a solvent for both TEOS and the ligand, a procedure which seemed to prevent phase separation and promote the ordering of the material.[12,25] The removal of excess template was carried out in a mild way with MeOH/aqueous HCl. The ratio of organic building block to TEOS which gave the best results in both preparations was 0.027:1.[12,24]

The powder XRD patterns of the materials prepared are presented in Figure 1. The diffractograms on the left refer to the MCM-41, PMS_1, and PMS_2 materials. The powder pattern of the calcined parent material MCM-41 clearly shows four reflections in the 2θ range 2–10°, which indexed to a

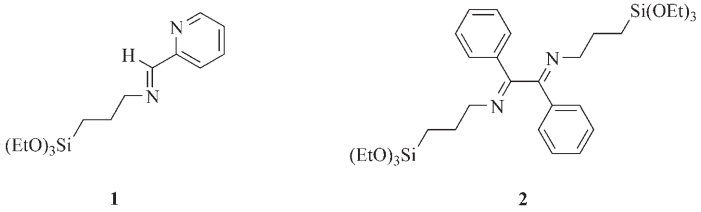

1 **2**

Scheme 1.

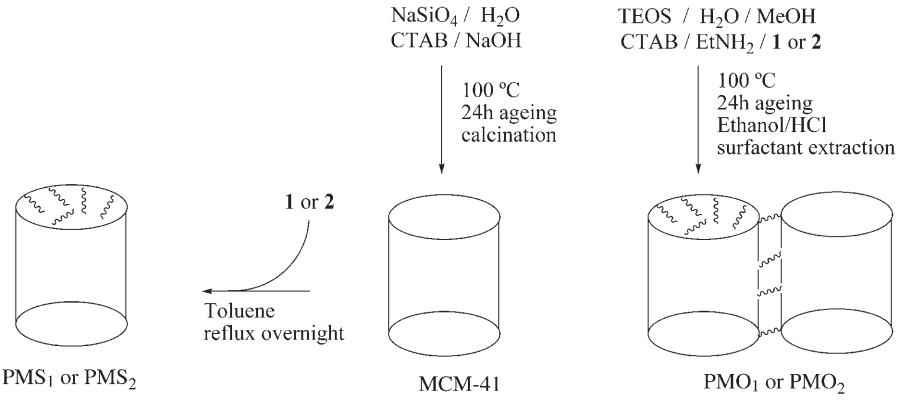

Scheme 2.

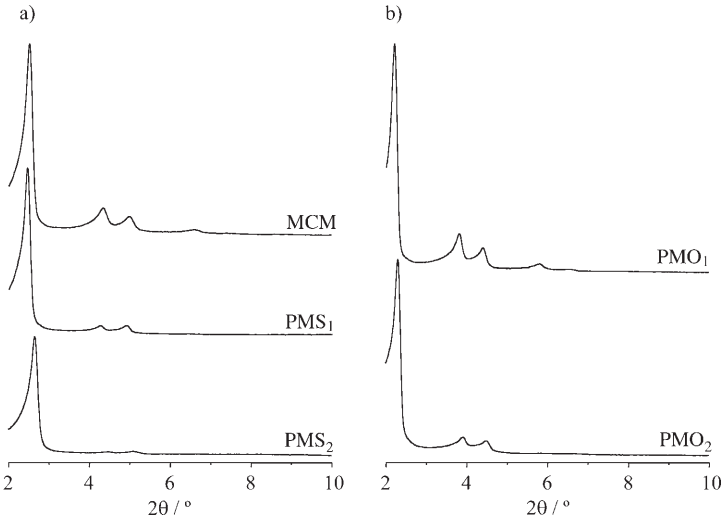

Figure 1. Powder XRD patterns of materials.

hexagonal cell as (100), (110), (200), and (210). The *d* value of the (100) reflection is 35.0 Å, corresponding to a lattice constant of $a = 40.4$ Å ($= 2d_{100}/\sqrt{3}$). Upon functionalization of the walls of the parent host material MCM-41 with ligands **1** or **2**, the powder patterns remain almost unchanged with regard to the positions of the peaks assigned to the characteristic reflections, suggesting the retention of the long-range hexagonal symmetry of the host material. However, a reduction of the peak intensities is clearly observed and was emphasized in the case of the PMS_2 material. This is not attributed to a loss of crystallinity, but rather to a reduction in the X-ray scattering contrast between the silica walls and pore-filling material.[26,27] The fact that this reduction occurs to a higher extent in PMS_2 than in PMS_1 is probably related with the building block **2** being bulkier than **1**.

In the case of the hybrid PMO_1 and PMO_2 materials, the patterns are more similar to those of the pure siliceous matrix MCM-41 parent material. Because the organic moieties are introduced during the preparation of the sol for subsequent ageing, the materials are thus obtained with a high degree of order compared to those of post-synthesis derivatization. It should also be noticed that PMO materials are template extracted, whereas those derived from MCM-41 (PMS_S) are template calcined. In some cases this may also account for the better defined powder XRD patterns shown by the PMO materials. Thus, the peak intensities of the corresponding powder XRD patterns are similar to those found for the parent MCM-41 material. This may be regarded as an indication that the organic moieties are indeed well integrated within the structure of the materials. Despite this, no further conclusions may be ruled out concerning the possible existence of poor or rich domains of organic moieties due to segregation of phases during the ageing process, a situation that is known to occur.[12,25] In the present case, however, this was minimized by the addition of methanol as solvent (see previous section).

Nitrogen adsorption studies at 77 K revealed that the pristine MCM-41 sample exhibits a reversible type-IV isotherm (Figure 2), characteristic of mesoporous solids (pore width between 2 and 50 nm, according to IUPAC).[28] The calculated textural parameters (S_{BET} and V_P) of this material agree with literature data (Table 1).[29,30] The capillary condensation/evaporation steps of the pristine MCM-41 sample

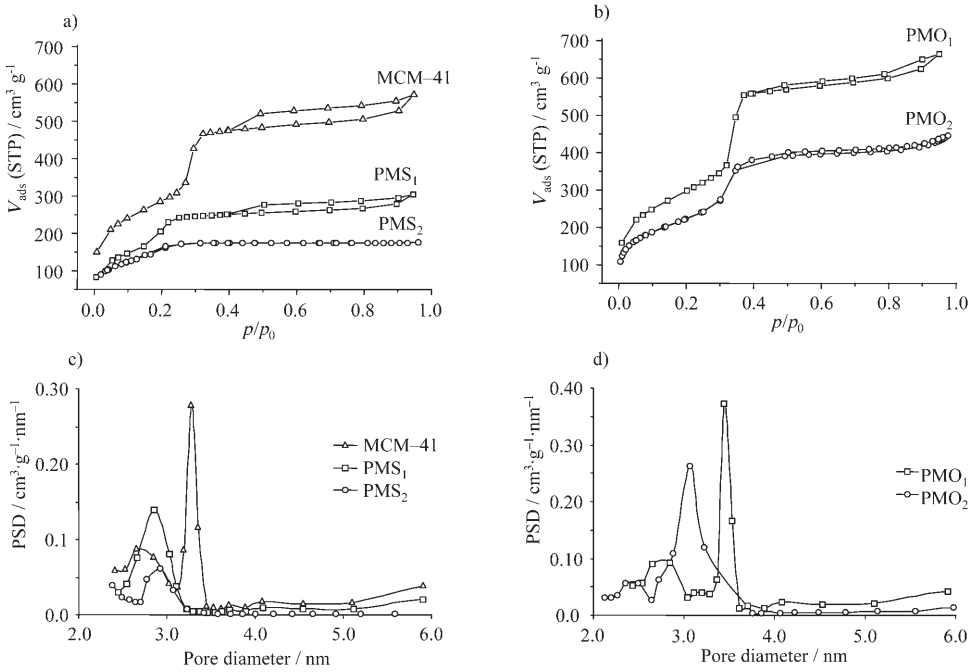

Figure 2. N_2 sorption isotherms at 77 K and pore size distribution (PSD) curves.

Table 1. Textural parameters for host and composite materials from N_2 isotherms at 77 K.

Sample	d_{100}[a] [Å]	S_{BET}[b] [m^2g^{-1}]	ΔS_{BET}[c] [%]	V_P[d] [cm^3g^{-1}]	ΔV_P[e] [%]	d_{BJH}[f] [nm]
MCM-41	35.0	1032	–	0.88	–	3.4
PMS_1	35.8	671	35	0.47	47	2.8
PMS_2	33.3	536	58	0.27	69	2.9
PMO_1	40.0	1069	–	1.03	–	3.8
PMO_2	38.6	803	–	0.69	–	2.9

[a] The d value of 100 XRD reflection. [b] Surface area according to BET isotherm. [c] Variation of surface area in relation to parent MCM-41. [d] Total pore volume at $p/p_0=0.95$. [e] Variation of total pore volume in relation to parent MCM-41. [f] Median pore width determined by the BJH method.

Table 2. Assignments and activities (DRIFT and FT Raman spectra) of the most active vibrational modes of silica-based matrix materials.

Assignment[a]	Wavenumber [cm^{-1}]	Major activity
νOH	3800–2500	IR
ν_{asym}SiOSi	1300–1000	IR
νSiO_d	980–940	IR and Raman
ν_{sym}SiOSi	850–800	IR and Raman
$\nu SiO+\delta OSiO$	600–550	IR and Raman
δSiOSi	425 and 270	Raman

[a] According to references [14] and [15].

appear in the 0.26–0.40 relative pressures range. The sharpness of this step reflects the uniform pore size.

The isotherms of the PMS_1 and PMS_2 functionalized materials revealed much lower N_2 uptake, accounting for decreases in s_{BET} (35 and 58%, respectively) and V_P (47 and 69%, respectively). These results suggest that immobilization of the ligands occurred on the internal silica surface (Figure 2, Table 1). This is also supported by the decrease of the p/p_0 coordinates of the inflection points of the isotherms upon post-synthesis treatment.[31] The height of the capillary condensation step, which is related to the volume of pore space confined by absorbate film on the pore walls, is much smaller in the case of the modified PMS_1 and PMS_2 materials. Furthermore, the maximum of the PSD curve (Figure 2) for MCM-41 determined by the BJH method, d_{BJH}, decreases from 3.4 to less than 3 nm (Table 1). The textural characterization of the PMO_1 and PMO_2 hybrid materials is similar to that of the MCM-41 material. Again, sharp steps (more evident in PMO_1) are observed, indicating a uniform pore size distribution.

Vibrational spectroscopy and local order effects: Vibrational spectra of silanol groups have been used to obtain valuable information about the local structure of materials.[17–21] In previous work the discussion focused on the study of the acidity of the hydroxy groups.[18] In particular, the νOH mode region can provide very rich data on "free" and "hydrogen-bonded" silanols, so that information about the nature of OH groups at the surface of the different materials can be inferred.

DRIFT (diffuse reflectance infrared fourier transform) spectra are particularly suited to record IR spectra of mesoporous materials, such as MCM-41, which are known to exhibit low mechanical resistance to the pressure required to prepare KBr pellets,[32,33] and contain reliable data on the local structure of porous inorganic matrix materials.[14,15] Table 2 summarizes the literature assignments of the most relevant modes for these materials.

The effects of pressure can be monitored by the band at approximately 570 cm^{-1} ($\nu SiO+\delta OSiO$, Table 2) which probes the mesoporous structure of the materials.[15] In our study, all the materials show a well-resolved intense band at 570 cm^{-1}, indicating that the non-rigid mesoporous structure is intact, as expected. Furthermore, this band was found to have a narrower profile in the PMO materials than in the others studied. This might indicate that the use of the organic building blocks may increase the quality of the local mesoporous structure, as will be discussed later in detail.

The DRIFT spectra for all materials are shown in Figure 3. Some clear differences are observed between the PMS and the corresponding PMO materials, in particular,

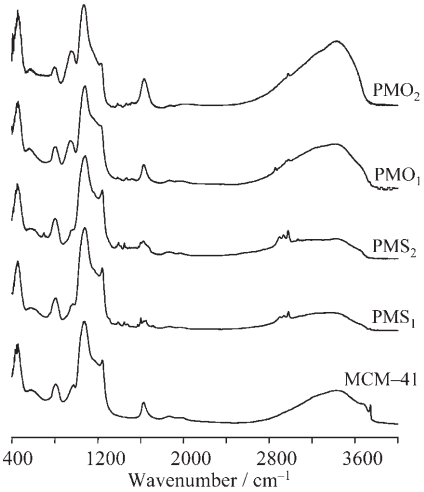

Figure 3. DRIFT spectra of MCM-41, PMS_1, PMS_2, PMO_1, and PMO_2 materials.

the bands corresponding to the νCH modes (about 3000 cm^{-1}) and the broad and intense band assigned to the νOH modes (3800–2500 cm^{-1}). Both the composite band assigned to the ν_{asym}SiOSi modes (1300–1000 cm^{-1}) and the framework modes region (intense group of bands in the 700–1400 cm^{-1} range), usually composed of several convoluted bands assigned to the different substructures made of tetrahedral SiO_4 units, provide a lot of information about the structural properties of siliceous materials, ranging from amorphous silica or aerogels/xerogels to zeolites to mesoporous structures.[14,34–37]

We start the analysis of the DRIFT spectra with the framework modes, which include the most intense group of bands with the maximum centered at around 1090 cm^{-1}. These were interpreted as a set of convoluted bands attributed to the ν_{asym}SiOSi modes arising from the elementary

tetrahedral SiO_4 units belonging to siloxane 4- and 6-ring substructures. These are hereafter denoted as $(SiO)_4$ and $(SiO)_6$, respectively. Other larger and smaller siloxane ring substructures are likely to occur, as well as other types of defects, but their statistical distribution may be neglected.

To characterize the local structure and differences between the materials in more detail, a deconvolution procedure was carried out for the group of bands in the 700–1400 cm^{-1} range. This was accomplished by fitting Gaussian profiles to the shape of the band, as shown in Figure 4. The best-fit procedure was achieved by considering a set of 4+2 Gaussian functions. This corresponds to four bands derived from the ν_{asym}SiOSi modes, centered at about 1240, 1180, 1080, and 1040 cm^{-1}, depending on the material. These components are indicative of the population distribution of $(SiO)_4$ and $(SiO)_6$ units within the framework of the materials. The remaining two bands centered at 960 and 800 cm^{-1} are assigned to the dangling (νSiO_d) and symmetric stretching modes (ν_{sym}SiO), respectively.[14] In some studies,[38] the band at 960 cm^{-1} was found to be convoluted with another weaker band at 900 cm^{-1}, which is assigned to νSiO modes. In our work, however, this band was not observed, and the use of a 4+3 set of Gaussian functions for the deconvolution procedure did not seem to improve the fitting results.

The results from the deconvolution procedure, summarized in Table 3, show some interesting features. The percentages of 6-ring units in the silica network, $\%(SiO)_6$, were obtained simply by adding $\%I$-[LO-$(SiO)_6$] and $\%I$-[TO-$(SiO)_6$]. Remember that LO and TO refer to the longitudinal-optic and transversal-optic components of the lattice (see Introduction) and belong to the ν_{asym}SiOSi mode. We provide another alternative.

Table 3. Results from the deconvolution of the ν_{asym}SiOSi modes of MCM-41, PMS_1, PMS_2, PMO_1, and PMO_2 materials by fitting of Gaussian functions.

		MCM-41	PMS_1	PMS_2	PMO_1	PMO_2
LO-$(SiO)_6$	center	1245	1244	1242	1236	1234
	FWHH	29.2	27.6	29.6	36.9	33.3
	$\%I$	5.5	5.6	5.8	6.9	7.5
LO-$(SiO)_4$	center	1182	1184	1178	1171	1164
	FWHH	116	108.3	123.6	105.8	93
	$\%I$	45.1	40.2	46.0	47.4	38.3
TO-$(SiO)_4$	center	1075	1077	1079	1076	1072
	FWHH	72	74.5	70.5	65.5	66
	$\%I$	43.6	47.3	37.3	40.4	50.0
TO-$(SiO)_6$	center	1033	1030	1028	1036	1038
	FWHH	35.2	38.7	47.1	36.7	32.4
	$\%I$	5.9	6.9	10.9	5.3	4.2
$\%(SiO)_6$[a]	$\%I$	11.4	12.6	16.8	12.2	11.7
νSiO_d	center	964	960	960	948	956
	FWHH	69.6	54.3	54.4	71.9	77.3
	$\%I$	14.6	10.6	10.7	29.4	40.6
ν_{sym}SiO	center	810	804	800	805	799
	FWHH	54.7	51.9	62.7	49.6	41.4
	$\%I$	14.6	14.3	21	13.6	7.8

[a] Based on the sum of $\%I$[LO-$(SiO)_6$] and $\%I$[TO-$(SiO)_6$].

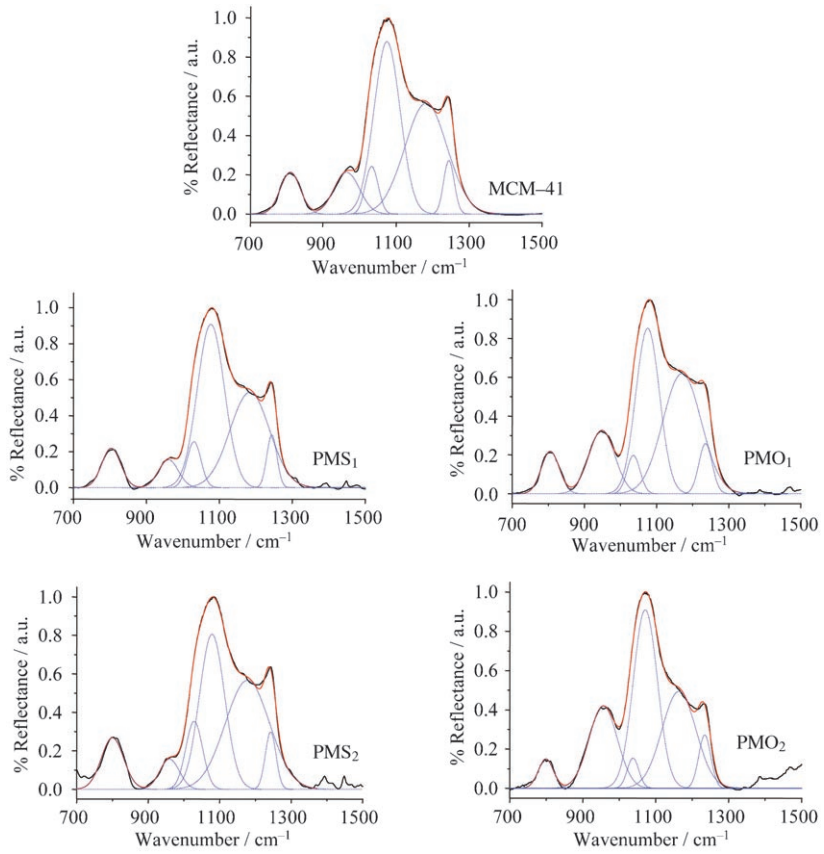

Figure 4. Results from deconvolution of the ν_{asym}SiOSi modes of MCM-41, PMS_1, PMS_2, PMO_1, and PMO_2 materials by fitting of Gaussian functions. Each curve shows the FTIR spectrum (black), deconvoluted bands (blue) and overall adjustment of deconvolution (red).

The first immediate observation is that both PMS materials do not present any noticeable structural change compared to the parent MCM-41 material. This result is expected, because the post-synthesis modifications should occur at the surface of the MCM-41 parent material without interfering to a large extent with the framework structure. For the PMO materials the situation is rather different. In this case, the bands are systematically red-shifted, with the exception of the TO-$(SiO)_6$ mode, which is blue-shifted. This may be explained by the influence that the position of some molecules from the organic ligands has on this partic-

ular mode. Therefore, steric hindrance may be a cause for the observed shift. By comparison, the corresponding LO-$(SiO)_6$ mode should not be influenced by this effect, considering that the vibration occurs in a direction where hindrance is not so relevant. Nevertheless, this is just one possible explanation and care is needed; for example, the TO-$(SiO)_4$ mode shows an ambiguous behavior.

Another relevant aspect is the full-width-at-half-height (FWHH) value found for these bands. There is little variation within each family of materials (MCM-41/PMS_1/PMS_2 and PMO_1/PMO_2), indicating that there are no significant changes in the local structure ordering of either $(SiO)_4$ or $(SiO)_6$ substructures.

We now analyze the νOH mode region of the DRIFT spectra, starting with the purely siliceous MCM, which shows two main features: A sharp band at 3747 cm^{-1} assigned to "free" OH groups and a broad band of high intensity centered at 3437 cm^{-1} corresponding to hydrogen-bonded hydroxy groups. It is expected that upon functionalization of the walls the sharp band will lose intensity to some extent or even disappear. Indeed, the disappearance of the sharp νOH feature and the decrease in intensity of the νOH broad band are evident in the νOH mode region of the FTIR spectra of both PMS_1 and PMS_2. These effects are consistent with a considerable functionalization of the walls. On the other hand, for PMO_1 and PMO_2, the intensity of the νOH band is considerably larger than in the parent MCM-41 material, suggesting an increase in the number of hydroxy groups compared to the number in MCM-41.

The framework band at 960 cm^{-1} is correlated with the number of hydroxy groups, which was also probed by the intensity of the broad band centered at approximately 3400 cm^{-1}. In this way it is possible to state that PMO_2 not only has the most intense νOH band of all the materials analyzed in the high wavenumber range, but also concomitantly exhibits the most intense band at 960 cm^{-1}, reflecting the relationship between the band intensity and hydroxy group population.

This population of hydroxy groups, an important feature of mesoporous materials, is roughly twice to four times higher for the PMO materials than for the other materials studied. Two possible explanations for this are: 1) the organic building blocks used in the synthesis of the PMO materials may lead to final materials with higher amounts of structural defects, thus yielding higher concentrations of terminal silanol groups; 2) the formation of interconnected mesochannels, as reported previously by Yuan and co-workers.[39] In their work, ammonia solution was used to create an interconnected three-dimensional structure starting from mesoporous MCM-41 with a pore-size distribution of 4 nm. The ammonia molecules randomly forced some of the silica walls to collapse, leading to larger holes. In the present work, $EtNH_2$ is used as a base, and the same may happen, with formation of an increased number of terminal silanol groups. A combination of the two could also be possible, which would account for the high degree of hydrophilicity in the PMO materials. In the case of the PMS_1 and PMS_2 materials, which were obtained after derivatization of the parent MCM-41 material with ligands **1** and **2**, respectively, it is reasonable to assume that these materials may have a different (lower) degree of hydrophilicity compared to that of the PMO materials.

As mentioned above, the population of hydroxy groups (see Figure 3) can be correlated with the intensity of the νSiO_d band centered at 950–960 cm^{-1} (Table 3) for the different materials. The degree of hydrophilicity of the sample can be measured by the proportion of the hydrophilic groups (hydroxy), [%(Si–O_d)], relative to the total silica network, and may be calculated by the following ratio of band areas [Eq. (1)]:

$$\%(\nu SiO_d) = 100 \times \frac{I(\nu SiO_d)}{I(\nu_{asym} SiOSi) + I(\nu SiO_d)} \quad (1)$$

Thus, the evolution of the ratio between the integrated area of the νOH modes and hydrophilicity correlates (see Table 3) with the overall hydrophilicity, as depicted in Figure 5.

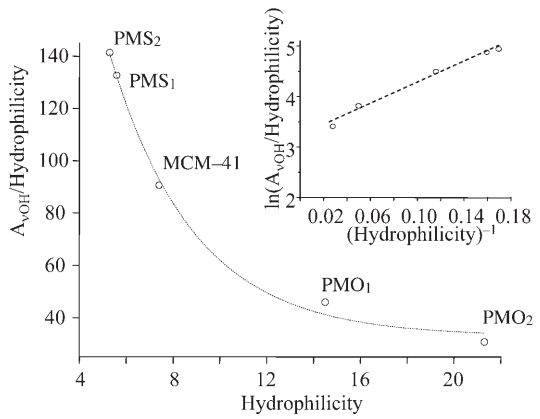

Figure 5. Correlation of the $I\nu_{OH}$/hydrophilicity versus hydrophilicity for the MCM-41, PMS_1, PMS_2, PMO_1, and PMO_2 materials. The dashed line is a fit of an exponential function ($r^2 = 0.99578$).

The results show that the method of introduction of the ligands, either by post-synthesis or by one-pot synthesis procedures, induces changes in the hydrophilicity of the materials. By looking at Figure 5 it is possible to observe that the PMS_2 material is the least hydrophilic of the series and that the PMO_2 material is the most hydrophilic one. Moreover, it is interesting to note that the same organic building block may afford materials with completely different characteristics.

In fact, the synthetic procedures (pairs PMS_1/PMO_1 or PMS_2/PMO_2) induce more significant changes in the hydrophilicity (see Figure 5) than the structural differences of the organic building blocks (having single or twin silylated branches, shown by the pairs PMS_1/PMS_2 and PMO_1/PMO_2). The inset in Figure 5 shows a linearization of the relationship indicating that the correlation is strong.

Raman spectroscopy offers another way of recording vibrational spectra of mesoporous materials without the necessity of any pressure treatment. Raman spectra of the materials under study (Figure 6) exhibit bands at around 980 cm^{-1} with medium intensity, assigned to the ν_{SiO} framework modes of the silanol groups, as in silica.[15]

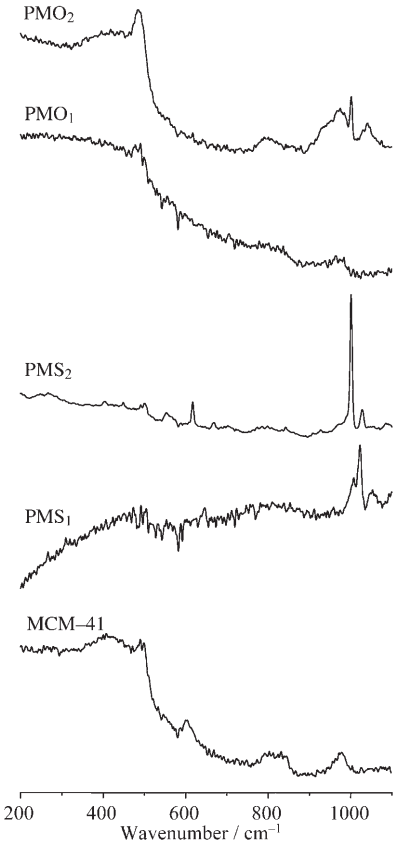

Figure 6. Raman spectra of MCM-41, PMS_1, PMS_2, PMO_1, and PMO_2 materials in the 200–1100 cm^{-1} range.

Other bands at 502 and 492 cm^{-1} may be associated with the perpendicular movement of bridging O atoms towards the bisecting line connecting two Si tetrahedral centers in a bridge. The position of the bands at around 492–502 cm^{-1} is thus related to the number of Si–O–Si bridges present in the materials.[15] The variation of the position of this band, observed for the different materials, is indicative of Si–O–Si bridges involved in annular structures of different orders.[40] In the present study, this band was observed at higher wavenumbers for the purely siliceous MCM related materials (MCM-41, PMS_1, and PMS_2) than for their hybrid matrix counterparts (PMO_1 and PMO_2). A plausible explanation for this may be that the incorporation of the larger organic molecules inside the matrix leads to the disruption of a given amount of Si–O–Si tetrahedral bridges, to adjust the matrix to the incorporated organic moieties. Thus, these modes should be less strained for the PMO materials than for their PMS counterparts.

The bands at 835, 605, 425, and 270 cm^{-1} with variable intensities throughout the series of materials analyzed can be assigned to modes of the siloxane bridges (835 and 270 cm^{-1}) and ring structure (605, 425 cm^{-1}) within the framework.

These observations support the results obtained from the corresponding DRIFT spectra, though they provide much less information in view of the poor quality of the spectra.

Pressure effects on the structure: The low mechanical stability of mesoporous materials, particularly those of the MCM-41 type, has been described,[32,33,41] and some authors have attempted to improve this property. For example, the use of trimethylsilyl groups as protective agents for residual silanols was described, resulting in a more hydrophobic material surface, which, in turn, increased moisture and mechanical stabilities in one step.[23] To evaluate the mechanical stability, measured by the behavior under pressure, samples of all the materials were pelletized, by pressing at 312 MPa for ten minutes. This pressure is near the value ((370 ± 74) MPa) reported to cause the total loss of the mesoporous structure.[33] Significant changes are indeed observed after pelletizing the materials. The intensity of the 100 peak in the powder XRD pattern decreases drastically, as observed in previous work.[32,33] The FTIR spectra also show a significant change in the overall profile of the spectra on going to the pelletized MCM-41 material (see Figure ESI1 in the Supporting Information), with a general broadening of the bands indicating a rise in the local disorder. Similar changes have been observed for all the remaining materials, PMS and PMO. A more detailed analysis of the FTIR spectra was carried out to compare the effects of pressure on the different materials, to detect changes in the local structure, and to understand which unit, $(SiO)_4$ or $(SiO)_6$, collapses to a larger extent. The same deconvolution procedure described above was used to inspect the framework bands region, based on a set of 4+2 Gaussian functions. The results are summarized in Table 4.

A comparison between the two sets of results (Tables 3 and 4) clearly shows that, despite a broadening (larger

Table 4. Results from deconvolution of the ν_{asym}SiOSi modes of MCM-41, PMS_1, PMS_2, PMO_1, and PMO_2 pelletized materials by fitting of Gaussian functions.

		MCM-41	PMS_1	PMS_2	PMO_1	PMO_2
$LO(SiO)_6$	center	1258	1248	1243	1243	1235
	FWHH	42.6	26.8	22.7	22.4	26.6
	%*I*	5.8	5.5	3.1	1.5	2.0
$LO(SiO)_4$	center	1147	1145	1140	1154	1170
	FWHH	58.4	58.7	59.5	53.7	78.1
	%*I*	17.7	19.3	24.2	14.1	21.7
$TO(SiO)_4$	center	1076	1075	1087	1105	1110
	FWHH	69.2	70.1	50	53.9	70.2
	%*I*	56.3	57.0	31.1	14.6	18.2
$TO(SiO)_6$	center	1030	1029	1042	1053	1047
	FWHH	52.8	52	57.8	78.1	84.5
	%*I*	20.2	18.2	41.7	69.8	58.1
$\%(SiO)_6$[a]	%*I*	26.0	23.7	44.7	71.4	60.1
νSiO_d	center	963	966	963	954	942
	FWHH	110	116.2	125.2	98.2	84.5
	%*I*	97.4	103.2	117.2	85.2	70.1

[a] Based on the sum of %*I*[LO-$(SiO)_6$] and %*I*[TO-$(SiO)_6$].

FWHH) observed for some bands, there is a systematic rise in the population of $(SiO)_6$ subunits for all the materials. Thus, $(SiO)_6$ subunits are more resistant and do not collapse under pressure so easily. Indeed, both $(SiO)_4$ and $(SiO)_3$ subunits are strained to some extent.[14] Under pressure, the smaller units react more easily with water molecules present in the mesopores, leading to their collapse and contributing to the concomitant increase of the relative population of $(SiO)_6$ subunits. On the other hand, the larger ring subunits are not as strained as the smaller ring subunits, being able to overcome the effect of pressure more efficiently, probably through a better capability of the $(SiO)_6$ subunits to adapt their conformation to the pressure conditions. As this increase in the proportion of $(SiO)_6$ subunits is observed for all the materials, without significant differences, the introduction of organic building blocks and the synthetic procedure do not affect the mechanical stability of the mesoporous matrix to a great extent.

Conclusion

The results reported show that differences at the local structure level of the same mesoporous materials obtained by using different synthetic procedures can be effectively probed by using vibrational spectroscopy. The materials with pure inorganic (siliceous) matrices, MCM-41, PMS_1, and PMS_2, exhibit a local structure that does not differ much from that of the materials with a hybrid matrix (PMO_1 and PMO_2). This is important as both methods have their advantages, and one would like to prevent phase segregation that may occur during the synthetic procedure used for PMO materials when mixing the organic building blocks with the silica source. Both the results discussed above, and those previously reported,[12,25] show that addition of a cosolvent, such as methanol, may be helpful in minimizing this problem. The statistical distribution of the local environments also exhibits a regularity in the values of the FWHH of the bands (see Table 3) for both the PMS and PMO materials. On the other hand, PMS_2 seems to be the only exception with regard to a larger contribution of the large $(SiO)_6$ subunits to the lattice. The twin-silylated branches may be responsible for secondary oligomerization reactions between neighboring molecules during the derivatization process of the MCM-41 surface. On the other hand, the template extraction methods are different for MCM-41/PMS materials (calcination) and for PMO materials (acidified solvent extraction), which could in fact lead to some differences among them. However, the aim of the work was to compare the materials that are obtained from normal preparation procedures.

More relevant differences between the two kinds of materials are found on analyzing the quality of the surface OH groups. Depending on the nature of the organic building blocks, the post-synthesis methods are known to contribute to the preparation of more hydrophobic surfaces in the systems. This occurs because of the reactions taking place at the derivatization stage which involve the free surface silanols. On the other hand, the co-condensation method between the same organic building block and the silica precursor leads in general to a more hydrophilic surface.[42,43] These ideas were confirmed because the hydrophilicity, measured by the νOH vibrations, and some associated framework modes were much larger in PMO_1 and PMO_2 than in MCM-41, PMS_1, and PMS_2. Therefore, one can control this property by choosing the method of synthesis.

Lastly, it was shown that the mechanical resistance of the materials was not affected to a great extent by any structural differences between the structures. Not even the introduction of organic building blocks within the mesoporous matrix seemed to have a great influence on the ability to prepare resistant PMO materials. The MCM-41-type materials have thin walls between the mesopores, but the introduction of the organic building blocks does not strengthen them.

This analysis of the local structure of mesoporous materials prepared by different approaches may be important when designing new materials for specific applications, such as sorbents or separating devices. Whereas most properties are similar (the material is essentially the same), some others, such as the hydrophilicity, will change significantly.

Experimental Section

General: All materials were obtained from Aldrich and used as received. Commercial grade solvents were dried and deoxygenated by standard procedures (Et_2O, THF, and toluene over Na/benzophenone ketyl; CH_2Cl_2 over CaH_2), distilled under nitrogen, and kept over 4 Å molecular sieves. Ligand **2** was synthesized as reported elsewhere.[12,13] Ligand **1** was prepared by adopting the same procedure and is described below in detail. MCM-41 and post-synthesis derivatized materials (PMS_1 and PMS_2) were synthesized as described previously by using $[(C_{16}H_{33})N(CH_3)_3]Br$ (CTAB) as templating agent.[23] Prior to the grafting experiment, physisorbed water was removed from calcined (813 K, for 6 h, under air) MCM-41 by heating at 453 K in a vacuum (10^{-2} Pa) for 2 h. Hybrid materials were also prepared by using ligands **1** or **2** according to a procedure reported in the literature with a load of approximately 3% organic material.[12] FTIR spectra were obtained as diffuse reflectance measurements (DRIFT) using 1 cm^{-1} resolution on a Nicolet 6700 spectrometer in the 400–4000 cm^{-1} range. Prior to all vibrational spectroscopy experiments, all the materials were activated to remove water. FT Raman samples were sealed in Kimax glass capillaries (id 0.8 mm) and spectra were obtained with 2 cm^{-1} resolution on a Bruker RFS-70 spectrometer equipped with a Nd-YAG laser by using an excitation wavelength of 1064 nm. Powder XRD measurements were obtained on a Philips PW1710 instrument by using CuK_α radiation filtered by graphite. The N_2 sorption measurements were obtained in an automatic apparatus (ASAP 2010; Micrometrics). BET specific surface areas (s_{BET}, p/p_0 from 0.03 to 0.13) and specific total pore volume, V_p ($p/p_0 = 0.95$) were estimated from N_2 adsorption isotherms measured at 77 K. The pore size distributions (PSD) were calculated by the BJH method by using the modified Kelvin equation with correction for the statistical film thickness on the pore walls.[44–46] The statistical film thickness was calculated by using the Harkins–Jura equation in the p/p_0 range from 0.1 to 0.95.

$C_5H_4NCH{=}N(CH_2)_3Si(OEt)_3$ (1): A solution of (3-aminopropyl)triethoxysilane (1.42 g, 6.4 mmol) in dry THF (10 mL) was added to a solution of pyridine-2-carboxaldehyde (0.69 g, 6.4 mmol) in dry THF, followed by 4 Å molecular sieves (0.6 g, 1.6 mm pellets), and a catalytic amount of $ZnCl_2$. After 12 h at 323 K the solution was filtered, and the resultant res-

idue rinsed with THF and the filtrate evaporated in vacuum to give the product as a pale yellow oil (3.98 g) in 85% yield.

^{1}H NMR (400.13 MHz, $CDCl_3$, 298 K, TMS): $\delta = 0.69$ (t, 2H; $SiCH_2$), 1.22 (t, 9H; OCH_2CH_3), 1.63–1.82 (m, 2H; $CH_2CH_2CH_2$), 1.98 (t, 2H; NCH_2), 3.81–3.87 (m, 6H; OCH_2CH_3), 7.57 (s, 1H; Ph), 7.91 (t, 2H; Ph), 8.42 (s, 1H; Ph), 8.74 ppm (s, 1H; Ph); ^{13}C{^{1}H} NMR (100.61 MHz, $CDCl_3$, 298 K, TMS): $\delta = 7.9$ ($SiCH_2$), 18.3 (OCH_2CH_3), 24.1 ($CH_2CH_2CH_2$), 58.4 (CH_2N), 64.1 (OCH_2CH_3), 121.3, 124.7, 136.6, 148.0, 149.7 (Ph), 161.9 ppm (HC=N); IR (KBr): $\tilde{\nu} = 2975$, 2927, 2885, 1651, 1626, 1598, 1570, 1481, 1457, 1442, 1390, 1368, 1348, 1304, 1281, 1191, 1167, 1102, 1079, 1027, 1018, 988, 958, 894, 882, 857, 781, 681, 660, 639, 546, 501, 475 cm^{-1}; elemental analysis calcd (%) for $C_{15}H_{26}O_3N_2Si$: C 58.02, N 9.02, H 8.44 ($r_{C/N} = 6.43$); found: C 58.35, N 9.19, H 8.48 ($r_{C/N} = 6.35$).

PMS_1: A solution of **1** (0.70 g, 1.13 mmol) in toluene (10 mL) was added to a suspension of MCM-41 (0.8 g) in toluene (10 mL) and the mixture heated at 100°C for 9 h. The resultant solid was then filtered off and washed four times with CH_2Cl_2 (4×15 mL), and dried in vacuum, at 50°C, for 3 h. ^{13}C CP/MAS NMR: $\delta = 8.8$ ($SiCH_2$), 16.2, 20.5, 41.6, 57.5, 128.1 ppm (Ph-C); ^{29}Si MAS NMR: $\delta = -55.4$ (T^1), -109.5 ppm (Q^4); ^{29}Si CP/MAS NMR: $\delta = -54.9$ (T^1), -59.6 (T^2), -67.0 (T^3), -91.9 (Q^2), -101.9 (Q^3), -109.2 ppm (Q^4); IR (KBr): $\tilde{\nu} = 3067$, 2978, 2927, 2891, 1652, 1494, 1447, 1390, 1245, 1080, 951, 800, 702 cm^{-1}; elemental analysis found (%): C 10.10, N 1.59, H 1.86 ($r_{C/N} = 6.35$).

PMO_1: An aqueous solution of ethylamine (3.46 mL, 52.8 mmol) was added to a stirred solution of CTAB (1.12 g, 3.08 mmol). Then a mixture of tetaethylorthosilicate (TEOS) (4.9 mL, 22 mmol) and **1** (0.19 g, 0.6 mmol) in methanol (1.78 mL) was added dropwise, leading to a composition in molar ratio of 1:0.027:0.14:2.4:2:100 SiO_2/**1**/CTAB/$EtNH_2$/MeOH/H_2O. The reaction mixture was stirred for a further 4 h at RT before being heated at 373 K for 24 h. The product was recovered by filtration, was washed thoroughly with distilled water, and was dried under ambient conditions. The surfactant was extracted by stirring 3.0 g of the synthesized hybrid material twice (to ensure maximum extraction) in 250 mL of methanol and 6.0 g of an aqueous solution of HCl (37%), at 323 K, for 6 h. The resulting solid was then filtered, washed with methanol and dried in air at 373 K. ^{13}C CP MAS NMR: $\delta = 8.3$ ($SiCH_2$), 20.5, 41.8, 47.8, 127 ppm (Ph-C); ^{29}Si MAS NMR: $\delta = -65.6$ (br d), -91.4, -100.7, -110.7 ppm; ^{29}Si CP MAS NMR: $\delta = -57.6$ (T^2), -66.1 (T^3), -91.6 (Q^2), -101.2 (Q^3), -110.8 ppm (Q^4); IR (KBr): $\tilde{\nu} = 3440$, 2978, 2959, 1971, 1886, 1652, 1630, 1571, 1472, 1387, 1230, 1082, 945, 805, 557, 457 cm^{-1}; elemental analysis found (%): C 3.29, N 0.51, H 1.28 ($r_{C/N} = 6.40$).

Acknowledgements

C.D.N. (SFRH/BPD/14512/2003), M.M.N. (SFRH/BD/18854/2004) and P.D.V. (SFRH/BPD/14903/2004) thank FCT for research grants.

[1] C. T. Kresge, M. E. Leonowicz, W. J. Roth, J. C. Vartuli, J. S. Beck, *Nature* **1992**, *359*, 710–712.
[2] J. S. Beck, J. C. Vartuli, W. J. Roth, M. E. Leonowicz, C. T. Kresge, K. D. Schmitt, C. T. W. Chu, D. H. Olson, E. W. Sheppard, S. B. McCullen, J. B. Higgins, J. L. Schlenker, *J. Am. Chem. Soc.* **1992**, *114*, 10834–10843.
[3] A. Taguchi, F. Schüth, *Microporous Mesoporous Mater.* **2005**, *77*, 1–45.
[4] D. M. Ford, E. E. Simanek, D. F. Shantz, *Nanotechnology* **2005**, *16*, S458–S475.
[5] S. R. Hall, C. E. Fowler, B. Lebeau, S. Mann, *Chem. Commun.* **1999**, 201–202.
[6] B. Hatton, K. Landskron, W. Whitnall, D. Perovic, G. A. Ozin, *Acc. Chem. Res.* **2005**, *38*, 305–312;
[7] W. J. Hunks, G. A. Ozin, *J. Mater. Chem.* **2005**, *15*, 3716–3724.
[8] H.-W. Jeong, C.-H. Kwak, Il-Kim, C.-S. Ha, S.-D. Seul, *Mol. Cryst. Liq. Cryst.* **2004**, *425*, 451–458.
[9] E. Besson, A. Mehdi, D. A. Lerner, C. Reye, R. J. P. Corriu, *J. Mater. Chem.* **2005**, *15*, 803–809.
[10] O. Olkhovyk, M. Jaroniec, *J. Am. Chem. Soc.* **2005**, *127*, 60–61.
[11] O. Olkhovyk, S. Pikus, M. Jaroniec, *J. Mater. Chem.* **2005**, *15*, 1517–1519.
[12] C. D. Nunes, P. D. Vaz, P. Brandão, J. Rocha, P. Ferreira, N. Bion, M. J. Calhorda, *Microporous Mesoporous Mater.* **2006**, *95*, 104–111.
[13] P. Ferreira, C. D. Nunes, P. D. Vaz, N. Bion, P. Brandão, J. Rocha, *Prog. Solid State Chem.* **2005**, *33*, 163–170.
[14] A. Fidalgo, L. Ilharco, *Chem. Eur. J.* **2004**, *10*, 392–398.
[15] E. Geidel, H. Lechert, J. Döbler, H. Jobic, G. Calzaferri, F. Bauer, *Microporous Mesoporous Mater.* **2003**, *65*, 31–42.
[16] G. A. Eimer, L. B. Pierella, G. A. Monti, O. A. Anunziata, *Catal. Lett.* **2002**, *78*, 65–75.
[17] A. Jentys, N. H. Pham, H. Vinek, *J. Chem. Soc. Faraday Trans.* **1996**, *92*, 3287–3291.
[18] J. Weglarski, J. Datka, H. He, J. Klinowski, *J. Chem. Soc. Faraday Trans.* **1996**, *92*, 5161–5164.
[19] A. Jentys, K. Kleestorfer, H. Vinek, *Microporous Mesoporous Mater.* **1999**, *27*, 321–328.
[20] V. A. Ermoshin, K. S. Smirnov, D. Bougeard, *Surfactant Sci. Ser.* **1996**, *368*, 147–151.
[21] K. Góra-Marek, J. Datka, *Appl. Cat A:* **2006**, *302*, 104–109.
[22] F. Hoffmann, M. Güngerich, P. J. Klar, M. Fröba, *J. Phys. Chem. C*, DOI: 10.1021/jp0668596.
[23] C. D. Nunes, M. Pillinger, A. A. Valente, J. Rocha, A. D. Lopes, I. S. Gonçalves, *Eur. J. Inorg. Chem.* **2003**, 3870–3877.
[24] M. Jia, A. Seifert, M. Berger, H. Giegengack, S. Schulze, W. R. Thiel, *Chem. Mater.* **2004**, *16*, 877–882.
[25] M. T. Anderson, J. E. Martin, J. G. Odinek, P. P. Newcomer, *Chem. Mater.* **1998**, *10*, 1490–1500.
[26] B. Marler, U. Oberhagemann, S. Voltmann, H. Gies, *Microporous Mater.* **1996**, *6*, 375–383.
[27] W. Hammond, E. Prouzet, S. D. Mahanti, T. J. Pinnavaia, *Microporous Mesoporous Mater.* **1999**, *27*, 19–25.
[28] S. J. Gregg, K. S. W. Sing in *Adsorption, Surface Area and Porosity*, 2nd ed., Academic Press, London, **1982**.
[29] M. D. Alba, A. Becerro, J. Klinowski, *J. Chem. Soc. Faraday Trans.* **1996**, *92*, 849–854.
[30] A. A. Romero, M. D. Alba, W. Zhou, J. Klinowski, *J. Phys. Chem. B* **1997**, *101*, 5294–5300.
[31] M. Kruk, M. Jaroniec, *Langmuir* **1999**, *15*, 5410–5413.
[32] N. Bai, Y. Chi, Y. Zou, W. Pang, *Mater. Lett.* **2002**, *54*, 37–42.
[33] K. Cassiers, T. Linssen, M. Mathieu, M. Benjelloun, K. Schrijnemakers, P. van der Voort, P. Cool, E. F. Vansant, *Chem. Mater.* **2002**, *14*, 2317–2324.
[34] F. L. Galeener, G. Lucovsky, *Phys. Rev. Lett.* **1976**, *37*, 1474–1478.
[35] S. W. de Leeuw, M. F. Thorpe, *Phys. Rev. Lett.* **1985**, *55*, 2879–2882.
[36] M. F. Thorpe, S. W. de Leeuw, *Phys. Rev. B* **1986**, *33*, 8490–8505.
[37] J. K. West, B. F. Zhu, Y. C. Cheng, L. L. Hench, *J. Non-Cryst. Solids* **1990**, *121*, 51–55.
[38] A. Chmel, E. K. Mazurina, V. S. Shashkin, *J. Non-Cryst. Solids* **1990**, *122*, 285–290.
[39] Z.-Y. Yuan, J.-L. Blin, B.-L. Su, *Chem. Commun.* **2002**, 504–505.
[40] O. Trofymluk, A. A. Levchenko, S. H. Tolbert, A. Navrotsky, *Chem. Mater.* **2005**, *17*, 3772–3783.
[41] C. D. Nunes, A. A. Valente, M. Pillinger, J. Rocha, I. S. Gonçalves, *Chem. Eur. J.* **2003**, *9*, 4380–4390.
[42] S.-J. Huang, S. Huh, P.-S. Lo, S.-H. Liu, V. S.-Y. Lin, *Phys. Chem. Chem. Phys.* **2005**, *7*, 3080–3087.
[43] J. He, Y. Xu, H. Ma, Q. Zhang, D. G. Evans, X. Duan, *J. Colloid Interface Sci.* **2006**, *298*, 780–786.
[44] E. P. Barrett, L. G. Joyner, P. P. Halenda, *J. Am. Chem. Soc.* **1951**, *73*, 373–380.
[45] M. Kruk, M. Jaroniec, *Langmuir* **1997**, *13*, 6267–6273.
[46] M. Kruk, V. Antochshuk, M. Jaroniec, *J. Phys. Chem. B* **1999**, *103*, 10679–10683.

Received: February 23, 2007
Published online: July 4, 2007

